INTERNATIONAL JOURNAL FOR NUMERICAL AND ANALYTICAL METHODS IN GEOMECHANICS
Int. J. Numer. Anal. Meth. Geomech., 2003; **27**:967–987 (DOI: 10.1002/nag.302)

A local identification technique for geotechnical and geophysical systems

Mourad Zeghal*,† and Caglar Oskay

Civil and Environmental Engineering Department, Rensselaer Polytechnic Institute, Troy, NY, 12180, U.S.A.

SUMMARY

Geotechnical structures and natural soil deposits are massive multi-phase particulate systems characterized by the development of localized response mechanisms under extreme loading conditions. Identification and analysis of such systems based on inverse boundary value problem formulations and sparse measurements are generally indeterminate. This paper presents an alternative local inverse problem technique. Point-wise identification analyses of the constitutive behaviour of water-saturated geotechnical and geophysical systems are performed using acceleration and pore pressure records provided by a cluster of closely spaced sensors. The developed novel technique does not require the availability of boundary condition measurements, or solution of an associated boundary value problem. The constitutive behaviour at a specific location of a soil-system is analysed independently of adjacent response mechanisms or material properties. Numerical simulations and centrifuge tests of a soil-retaining wall system are used to demonstrate the capabilities of the developed technique. Copyright © 2003 John Wiley & Sons, Ltd.

KEY WORDS: system identification; inverse problem; soil dynamics; constitutive modelling; centrifuge test

1. INTRODUCTION

Geotechnical structures and natural soil deposits are massive systems which have distributed parameters and state. Some deposits are in fact semi-infinite and have no well-defined boundaries. Geotechnical systems generally exhibit a broad range of response patterns when subjected to dynamic loading conditions [1–3]. Some of these patterns reflect local mechanisms associated with the particulate nature of soils, and others are related to abrupt changes in properties. Soil constitutive models have reached high levels of refinement and sophistication e.g. Reference [4] in view of drastic improvements in computational tools over the last decades. However, these models generally have limited predictive capabilities for severe loading conditions if they have not been properly benchmarked [5]. Soil sample experiments (e.g. triaxial tests) have been widely used to calibrate the constitutive relations of geotechnical systems. Nevertheless, because of limitations in reproducing *in situ* stress and pore-fluid conditions, the

*Correspondence to: M. Zeghal, Civil and Environmental Engineering Department, Rensselaer Polytechnic Institute, Troy, NY, 12180, U.S.A.
†E-mail: zeghal@rpi.edu

Contract grant sponsor: National Science Foundation; contract/grant number: CMS 9984754

Received 18 April 2003
Revised 14 May 2003

consensus is that these experiments may not fully reflect reality. System identification and inverse problem analyses using seismic records of full-scale systems as well as centrifuge models are starting to play an important role in development as well as calibration and validation of soil models.

Early monitoring efforts of the seismic response of soil systems consisted of measuring accelerations along a free surface and when possible at an input boundary. Vertical (downhole) array instrumentation have been employed to monitor level sites since the 1950s in the United States and Japan. A significant number of sites and embankments has been instrumented with such arrays over the last 2 decades, and some of these arrays included pore pressure sensors [6–8]. The current state-of-the-art in centrifuge model testing also relies on vertical arrays of acceleration and pore-pressure sensors [2]. Such instrument configurations monitor a soil-system response at sparse locations. Identifying and calibrating models of the dynamic constitutive response of a system using experimental data provided by sparse arrays is a challenging task, especially when the behaviour of this system is marked by the development of localized mechanisms (e.g. liquefaction or formation of shear bands). The problem is complicated further in the absence of well-defined boundary conditions, such as for semi-infinite systems. Historically, the complexity of soil behaviour and scarcity of adequate data had hindered the adoption of system identification methods in geotechnical model development and calibration, and only a limited number of studies has been undertaken in this regard e.g. Reference [9].

The particulate non-cemented characteristic of soil deposits allows easy instrumentation of new and existing geotechnical systems with dense arrays of a new generation of miniature accelerometer, inclinometer, and pore-water pressure transducers (some of which are micro-electro-mechanical system or MEMS [10,11]). In view of their small size, these sensors may be installed virtually at any location within a system and along its boundaries without compromising its structural integrity. Nevertheless, a thorough monitoring of massive geotechnical and geophysical systems is generally unpractical and costly. Furthermore, the boundary conditions of semi-infinite systems (such as sites) subjected to earthquake excitations will only be partially available at best. This paper presents a point-wise system identification technique for analyses of the dynamic response of distributed soil systems using local arrays of acceleration and pore-water pressure sensors. The developed technique is particularly advantageous in investigations of semi-infinite soil systems or in the presence of local response mechanisms. In the following sections, a general formulation of the identification approach is described for cohesionless and cohesive soils. Results of the conducted identification analyses are presented thereafter.

2. FORWARD PROBLEM

Saturated geotechnical systems consist of mixtures of mineral particles, forming a porous matrix, and fluids (water and possibly others) filling the pores. These systems exhibit a broad range of response patterns depending on confining pressure and level of deformation, as well as pore fluid pressures [2,3]. Continuum models based on the mixture theory or Biot's formulations have been used to describe the response of granular soils. These models result in a full coupling of the pressure and velocity fields of the water (fluid) phase with the displacement and deformation fields of the solid skeleton. This study is based on the simplified, $\mathbf{u}$–p model which presumes that the effects of the fluid motion relative to the solid particles are negligible. Such a

model is adequate for the relatively low frequency input motions which prevail during seismic excitations. The coupled 2-phase model is given by [4,12]

Field equations: ($\forall \mathbf{x} \in \Omega$)

$$(\boldsymbol{\sigma}' + p_{\mathrm{w}}\boldsymbol{\delta}).\boldsymbol{\nabla} + \rho\mathbf{g} = \rho\ddot{\mathbf{u}} \tag{1}$$

$$(\rho_{\mathrm{w}}\mathbf{K}\mathbf{g}).\boldsymbol{\nabla} + g\rho_{\mathrm{w}}\left(\dot{\boldsymbol{\varepsilon}} : \boldsymbol{\delta} + \frac{\dot{p}_{\mathrm{w}}}{Q}\right) = (\mathbf{K}(p_{\mathrm{w}}\boldsymbol{\nabla} + \rho_{\mathrm{w}}\ddot{\mathbf{u}})).\boldsymbol{\nabla} \tag{2}$$

$$\mathrm{d}\boldsymbol{\sigma}' = \mathrm{d}\boldsymbol{\sigma}'(\mathrm{d}\boldsymbol{\varepsilon}, \mathrm{d}\dot{\boldsymbol{\varepsilon}}, \ldots) \tag{3}$$

Boundary conditions:

$$\mathbf{u}(\mathbf{x}, t) = \bar{\mathbf{u}}(\mathbf{x}, t) \quad (\forall \mathbf{x} \in \Gamma_u) \tag{4}$$

$$\boldsymbol{\sigma}.\mathbf{n} = \bar{\boldsymbol{\tau}}(\mathbf{x}, t) \quad (\forall \mathbf{x} \in \Gamma_\sigma) \tag{5}$$

$$p_{\mathrm{w}}(\mathbf{x}, t) = \bar{p}_{\mathrm{w}}(\mathbf{x}, t) \quad (\forall \mathbf{x} \in \Gamma_{\mathrm{p}}) \tag{6}$$

Initial conditions: ($\forall \mathbf{x} \in \Omega$)

$$\mathbf{u}(\mathbf{x}, 0) = \mathbf{u}_0(\mathbf{x}) \tag{7}$$

$$\dot{\mathbf{u}}(\mathbf{x}, 0) = \dot{\mathbf{u}}_0(\mathbf{x}) \tag{8}$$

$$p_{\mathrm{w}}(\mathbf{x}, 0) = p_{\mathrm{w}0}(\mathbf{x}) \tag{9}$$

in which t is time variable (a superposed dot denotes a material time derivative), $\mathbf{x} = \{x_1, x_2, x_3\}^{\mathrm{T}}$ refers to location within a Cartesian co-ordinate system, $\boldsymbol{\nabla} = \{\partial/\partial x_1, \partial/\partial x_2, \partial/\partial x_3\}^{\mathrm{T}}$ is vector differential operator, p_{w} is pore-water pressure, $\boldsymbol{\sigma}'$ is effective stress tensor, $\boldsymbol{\varepsilon}$ is strain tensor, $\boldsymbol{\delta}$ is Kronecker delta unit tensor, $\mathbf{u}$ is displacement vector of the solid phase, $\mathbf{g}$ is gravity force vector (g is gravitational acceleration), $\mathbf{K}$ is permeability tensor, Q is equivalent (soil–water) bulk modulus, ρ and ρ_{w} are mass densities of the saturated soil and water, respectively, $\bar{\mathbf{u}}$ is prescribed boundary displacement (input motion), $\bar{\boldsymbol{\tau}}$ is prescribed boundary traction, $\mathbf{n}$ is unit outward normal vector, $\bar{p}_{\mathrm{w}}$ is prescribed boundary water pressure, $\mathbf{u}_0$ and $\dot{\mathbf{u}}_0$ are initial displacement and velocity, $p_{\mathrm{w}0}$ is initial pore-water pressure distribution, Ω is a geometrical model of the soil-system domain (Figures 1 and 2), Γ_u and Γ_σ are displacement and traction boundaries, and Γ_{p} is pore-water pressure boundary. The forward boundary value problem of the dynamic response of soil systems (represented by Equations (1)–(9)) have been widely solved numerically using the finite element method e.g. Reference [4].

3. LOCAL IDENTIFICATION

Identification of the non-linear constitutive behaviour of massive soil systems based on inverse analyses of the above boundary value problem (Equations (1)–(9)) is a significant analytical and computational challenge. Geotechnical systems are generally stratified deposits with local variabilities in stiffness and strength properties. Under severe loading conditions these systems may exhibit localized response mechanisms, such as liquefaction or formation of shear bands (as shown schematically in Figures 1 and 2). Earthquake case histories and centrifuge experiments strongly suggest that such local variations in properties and mechanisms may have significant

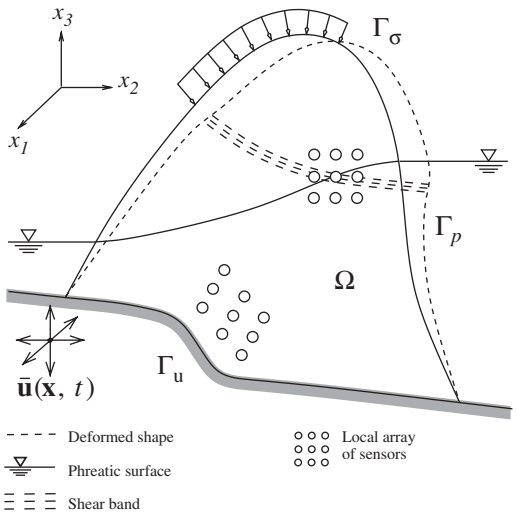

Figure 1. Schematic of the forward problem of a soil-system subjected to seismic excitations.

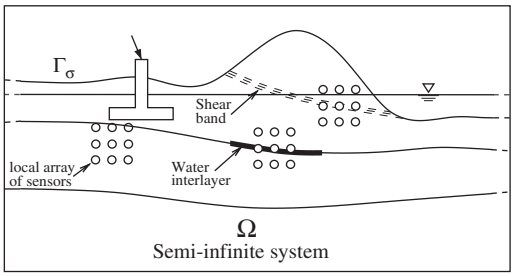

Figure 2. Schematic of a semi-infinite soil system showing a range of conditions which may be analysed advantageously using local identification techniques.

impact on the global behaviour and performance of massive soil systems [2,3]. A substantially large number of sensors would generally be needed to fully monitor the global and local response mechanisms of the solid and fluid phases as well as the boundary conditions of such systems. The problem is even more complex for semi-infinite systems where the seismic source and associated boundaries are unknown. Adequate monitoring of the boundary conditions of these systems (when subjected to seismic excitations) remains an unresolved issue.

Global identification analyses of the seismic response of distributed systems using boundary value problem formulations and information provided by a limited number of sensors (installed at sparse locations within the system and along the boundary) are commonly indeterminate. Data recorded by these sensors are generally sufficient to estimate only the global response features, and do not provide enough information to identify a unique and physically realistic model capable of accurately describing all involved response mechanisms. Consequently, global identifications usually fail to capture local properties and response mechanisms, and average their effects over the whole system domain. The problem was therefore addressed using an

alternative local approach. A novel point-wise identification methodology and technique were developed to analyse the response of soil-systems locally using the motions and pore-pressures recorded by multi-dimensional dense arrays (clusters) of accelerometers and pressure sensors. The developed technique does not require recordings of boundary conditions or solution of an associated boundary value problem. The identification problem of saturated 2-phase soils is reduced to a single solid phase analysis by using the concept of effective stresses and local measurements of pore-water pressure (in addition to acceleration).

3.1. Algorithm

The developed local identification technique consists of: (1) estimation of strain tensor time histories (Section 3.2) using the motions recorded by a cluster of instruments (arranged in appropriate multidimensional configurations), (2) evaluation of stress tensors corresponding to the estimated strains employing a pre-selected class of constitutive models of soil response (Section 3.3), (3) computation of accelerations associated with the estimated stresses and recorded pore-water pressures utilizing the equilibrium equations (Section 3.4), and (4) evaluation and calibration of an optimal model of soil response by minimizing the discrepancies between recorded and computed accelerations (Section 3.5). In steps (1) and (3), discrete differentiation tools were employed to evaluate strain tensor-time histories from displacement records, and to obtain accelerations corresponding to the computed stresses. Figure 3 displays a flowchart of the developed algorithm.

3.2. Evaluation of strains

For small deformations, the strain tensor, $\boldsymbol{\varepsilon}$, is given by

$$\boldsymbol{\varepsilon} = \tfrac{1}{2}(\mathbf{u}\nabla + \nabla\mathbf{u}) \tag{10}$$

When a soil system is monitored by an array consisting of a cluster of closely spaced accelerometers, estimates of the strain field may be evaluated within the instrumented zone using

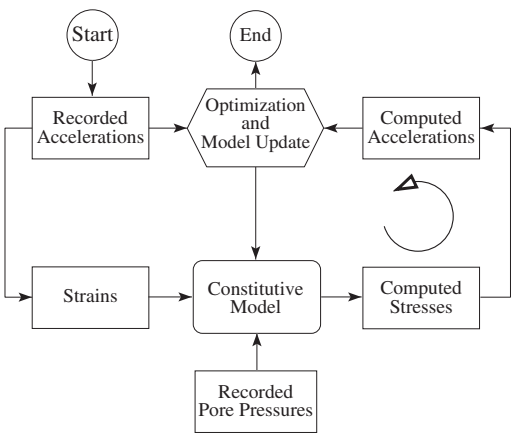

Figure 3. Algorithm of proposed local identification technique of saturated soil systems (using a $\mathbf{u}$–p formulation).

displacements obtained through double time integration of acceleration records along with finite differentiation [13] or other interpolation techniques. The accuracy of these strain estimates is a function of spacing, number of measurements used in interpolations, and involved motion wavelengths (Section 4.2). For a 3-D analysis, second order accurate estimates may be obtained utilizing the 3-D motions provided by a group of 7 accelerometers appropriately distributed along the x_1, x_2, and x_3 directions, as shown in Figure 4. For instance, the strain tensor at the (p,q,r) instrument location of Figure 4 may be estimated using a central difference scheme:

$$\boldsymbol{\varepsilon}^{(p,q,r)} = \tfrac{1}{2}(\mathbf{u}\boldsymbol{\nabla}^{(p,q,r)} + \boldsymbol{\nabla}^{(p,q,r)}\mathbf{u}) \tag{11}$$

in which p, q and r refer to a 3-index position numbering, and $\boldsymbol{\nabla}^{(p,q,r)}$ is a discrete counterpart of the differential operator $\boldsymbol{\nabla}$ at the (p,q,r) location:

$$\boldsymbol{\nabla}^{(p,q,r)}(.) = \begin{Bmatrix} \dfrac{(.)^{(p+1,q,r)} - (.)^{(p-1,q,r)}}{2\Delta x_1} \\ \dfrac{(.)^{(p,q+1,r)} - (.)^{(p,q-1,r)}}{2\Delta x_2} \\ \dfrac{(.)^{(p,q,r+1)} - (.)^{(p,q,r-1)}}{2\Delta x_3} \end{Bmatrix} \tag{12}$$

Equation (12) presumes constant instrument spacings, Δx_1, Δx_2, and Δx_3 in the x_1, x_2, and x_3 directions, respectively. Alternative expressions may be employed with nonuniform spacings [13,14]. A larger number of sensors is needed to achieve higher order accuracies (13 are required for a 4th order accurate 3-D analysis). Within the developed local identification technique, the strain estimates are employed along with a class of constitutive soil models to evaluate the associated stresses (Section 3.3). These stresses are subsequently used to compute the corresponding accelerations, as described in Section 3.4. Thus, a minimum of 19 accelerometers distributed within an orthogonal (3-by-3-by-3) parallelepiped arrangement are required to evaluate the strains at the 6 central locations of the configuration facets using 2nd order accurate forward and backward difference approximations (Fig. 4). The stresses corresponding to these strains are then used to evaluate accelerations at the central (p,q,r) location of the

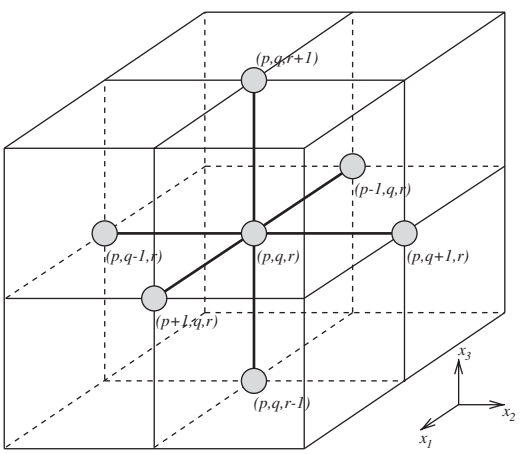

Figure 4. Basic orthogonal configuration of accelerometers required to evaluate second order accurate strains at a (p,q,r) location based on the classical central difference technique.

cluster (Fig. 4). For saturated cohesionless soils, six additional sensors are required to monitor the pore pressure at the central locations of the configuration facets (where strains are estimated). Such an identification procedure was found to be quite sensitive to errors associated with forward and backward differentiations. Furthermore, installing pore pressure sensors and accelerometers at the same exact locations (facet central points) may not be technically possible.

This paper presents two alternative procedures in which arrays of 7 and 19 accelerometers uniformly distributed within a general skew-rectilinear (or orthogonal) parallelepiped configurations (Figure 5) are used to achieve first and second order accurate 3-D analyses, respectively. The strains are evaluated at 6 of the 8 intermediate central locations $(p-\frac{1}{2}, q-\frac{1}{2}, r-\frac{1}{2})$ to $(p+\frac{1}{2}, q+\frac{1}{2}, r+\frac{1}{2})$ of the accelerometer array (Figures 5 and 6). For saturated cohesionless soils, the identification technique requires pore pressure measurements at these six intermediate central locations. Figure 7 displays the sensor configuration scheme for first and second order accurate 2-D analyses (the strains are evaluated and pore-water pressures are measured at the four intermediate locations $(p-\frac{1}{2}, q-\frac{1}{2})$ to $(p+\frac{1}{2}, q+\frac{1}{2})$).

First order accurate estimate of the strain tensor at the $(p+\frac{1}{2}, q+\frac{1}{2}, r+\frac{1}{2})$ intermediate central location, for instance, may be evaluated in a x'_i skew rectilinear co-ordinate system (Figure 5) using the finite difference operator:

$$\nabla_{x'}^{(p+\frac{1}{2},q+\frac{1}{2},r+\frac{1}{2})}(.)_{x'} = \begin{Bmatrix} \dfrac{(.)_{x'}^{(p+1,q,r)} - (.)_{x'}^{(p,q,r)}}{\Delta x'_1} \\ \dfrac{(.)_{x'}^{(p,q+1,r)} - (.)_{x'}^{(p,q,r)}}{\Delta x'_2} \\ \dfrac{(.)_{x'}^{(p,q,r+1)} - (.)_{x'}^{(p,q,r)}}{\Delta x'_3} \end{Bmatrix} \tag{13}$$

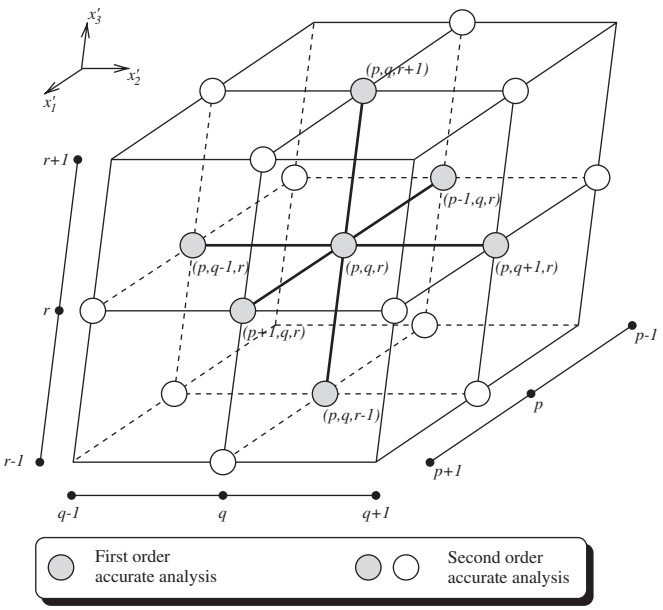

Figure 5. Skew-rectilinear configuration of accelerometers used in first and second order accurate local 3-D identification analyses.

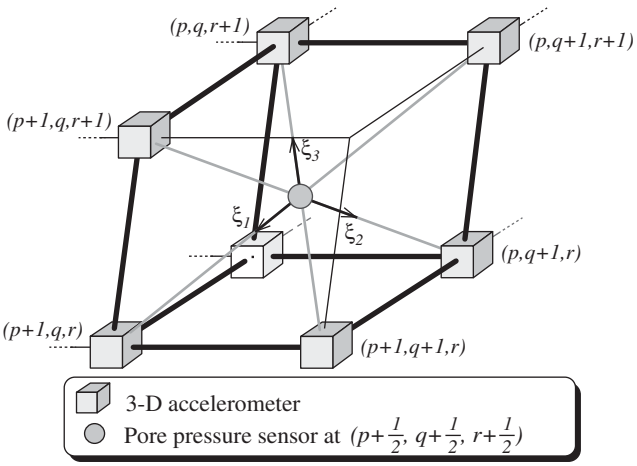

Figure 6. Detailed view of sensors used to estimate strains at the $(p+\frac{1}{2}, q+\frac{1}{2}, r+\frac{1}{2})$ location and associated skew-rectilinear co-ordinate system, ξ_i.

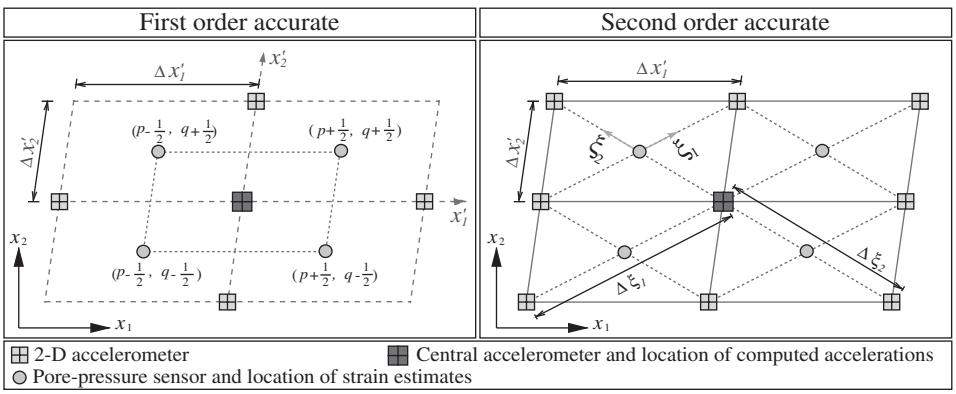

Figure 7. Instrument array configuration for first and second order accurate 2-D analyses.

and the motions recorded by the instruments at (p,q,r), $(p+1,q,r)$, $p,q+1,r)$, and $(p,q,r+1)$ locations of Figure 5. Analogous expressions may be used to evaluate the strain at other intermediate locations. Second order accurate strains were evaluated in terms of the skew rectilinear co-ordinates ξ_i $(i=1,2,3)$ shown in Figure 6. For example, strains at the intermediate $(p+\frac{1}{2}, q+\frac{1}{2}, r+\frac{1}{2})$ location were estimated using the motion recorded by the $(p+1,q,r)$, $(p,q+1,r)$, $(p,q,r+1)$, $(p+1,q+1,r)$, $(p,q+1,r+1)$, and $(p+1,q,r+1)$ instruments. At these intermediate locations, the strain tensor is given by [15]

$$\boldsymbol{\varepsilon} = \boldsymbol{\Phi}_{x-\xi}\boldsymbol{\varepsilon}_{\xi}\boldsymbol{\Phi}_{x-\xi}^{-1} \tag{14}$$

in which $\boldsymbol{\varepsilon}_{\xi}$ is strain tensor in the skew rectilinear co-ordinate system ξ_i (Figure 6):

$$\boldsymbol{\varepsilon}_{\xi} = \tfrac{1}{2}(\mathbf{u}_{\xi}\boldsymbol{\nabla}_{\xi} + \boldsymbol{\nabla}_{\xi}\mathbf{u}_{\xi}) \tag{15}$$

In Equations (14) and (15), $\mathbf{u}_\xi$ and $\mathbf{V}_\xi = \{\partial/\partial\xi_1, \partial/\partial\xi_2, \partial/\partial\xi_3\}^{\mathrm{T}}$ are displacement and differential vectors expressed in the skew co-ordinate system ξ_i, and $\mathbf{\Phi}_{x-\xi}$ is the transformation tensor from the skew rectilinear to the Cartesian co-ordinate system [15]:

$$[\mathbf{\Phi}_{x-\xi}]_{ij} = \frac{\partial x_j}{\partial \xi_i}, \quad i, j = 1, 2, 3 \tag{16}$$

The corresponding stresses obtained at these same intermediate locations (Section 3.3) are then used to evaluate second order accurate accelerations (Section 3.4) at the central location of the cluster (Figure 5).

3.3. Constitutive modelling and estimation of stresses

Non-parametric estimates of stresses may be computed directly from recorded accelerations only for simple systems and loading conditions, such as a level site subjected to vertical seismic wave propagation [16]. Conversely, distributed soil-systems are generally statically indeterminate, and constitutive modelling is necessary to evaluate stress tensors corresponding to the strains estimated in Section 3.2. Two classes of visco-elasto-plastic stress–strain models were therefore selected to idealize soil dynamic response. A Drucker–Prager model was used to describe the pressure dependent behaviour of granular cohesionless soils, while a Von-Mises model was used in analyses of short term response of clayey media. A multi-surface plasticity technique was used to model the non-linear, hysteretic and path dependent stress–strain response of soils and address the problem of load reversal associated with dynamic excitations [17]. The elasto-plastic constitutive model for a saturated cohesionless granular soil is given by [18]

Yield function:

$$f(\boldsymbol{\sigma}, \boldsymbol{\alpha}, M) = 3/2(\mathbf{S}' - p'\boldsymbol{\alpha}) : (\mathbf{S}' - p'\boldsymbol{\alpha}) - (Mp')^2 = 0 \tag{17}$$

Flow rule:

$$\mathrm{d}\boldsymbol{\varepsilon}^{\mathrm{p}} = \langle \mathrm{d}L \rangle \mathbf{P} \tag{18}$$

Hardening rule:

$$\mathrm{d}\boldsymbol{\alpha} = \langle \mathrm{d}L \rangle a\boldsymbol{\mu} \tag{19}$$

$$\mathrm{d}M = \langle \mathrm{d}L \rangle b \tag{20}$$

in which $\mathbf{S}' = \boldsymbol{\sigma}' - p'\boldsymbol{\delta}$ is deviatoric effective stress tensor, $p' = \frac{1}{3}\mathrm{trace}(\boldsymbol{\sigma}')$ is mean effective confining pressure, $\boldsymbol{\alpha}$ and M are plastic internal variables defining location and size of the yield surface, ':' denotes the scalar product of two second order tensors, $\mathrm{d}\boldsymbol{\varepsilon}^{\mathrm{p}}$ is plastic strain tensor, $\mathbf{P}$ is a symmetric second order tensor giving the direction of plastic deformations, a is kinematic hardening parameters, $\boldsymbol{\mu}$ is second order tensor defining the direction of kinematic hardening [17], b is isotropic hardening parameter (a purely kinematic hardening rule was used in this study), $\langle\ \rangle$ are Mac-Cauley brackets ($\langle \mathrm{d}L \rangle = \mathrm{d}L H(\mathrm{d}L)$, with H the heaviside step function), and $\mathrm{d}L$ is plastic loading function increment: $\mathrm{d}L = \mathbf{Q} : \mathrm{d}\boldsymbol{\sigma}'/H_{\mathrm{p}}$ (in which $\mathbf{Q}$ is outward normal to the yield surface, and H_{p} is plastic modulus). The visco-elasto-plastic constitutive equation may then be expressed as [4,17]

$$\mathrm{d}\boldsymbol{\sigma}' = \left(\mathbf{E} - \frac{(\mathbf{E} : \mathbf{P})(\mathbf{Q} : \mathbf{E})}{H_{\mathrm{p}} - H_0} \right) : \mathrm{d}\boldsymbol{\varepsilon} + \zeta \mathrm{d}\dot{\boldsymbol{\varepsilon}} \tag{21}$$

in which $\mathbf{E}$ is elastic constitutive tensor (as a function of the soil elastic shear modulus, G_0 and Poisson's ratio, v), $H_0 = \mathbf{Q} : \mathbf{E} : \mathbf{P}$, and ζ is viscous damping factor. A viscous damping mechanism was used to supplement the purely hysteretic (material) energy dissipation which commonly fails to account for soil low-strain damping observed in case history investigations [19]. The deviatoric plastic flow is selected to be associative, while a non-associative rule is used for the volumetric component to accommodate both contractive and dilative behaviours [4,18]. The volumetric flow rule suggested in Reference [18] was adopted in this study:

$$\text{trace}(\mathbf{P}) = \frac{3\mathbf{S}' : \mathbf{S}' - 2(\bar{\eta} p')^2}{3\mathbf{S}' : \mathbf{S}' + 2(\bar{\eta} p')^2} \tag{22}$$

in which $\bar{\eta}$ is material parameter associated with the transition from a contractive to a dilative behaviour.

The short term yield conditions of clayey soils are independent of confining pressures, and may be expressed in terms of total stress tensor $\boldsymbol{\sigma}$ using the Von-Mises criterion: $f(\boldsymbol{\sigma}, \boldsymbol{\alpha}, k) = 3/2(\mathbf{S} - \boldsymbol{\alpha}) : (\mathbf{S} - \boldsymbol{\alpha}) - k^2 = 0$ (in which $\mathbf{S}$ is deviatoric stress tensor and k is plastic internal variable defining the size of the yield surface). Under short term loading conditions, clayey materials exhibit mostly an associative flow rule ($\mathbf{P} = \mathbf{Q}$). The corresponding constitutive equation is similar to Equation (21), and given in terms of total stresses.

3.3.1. Recognition of the most consequential parameters. The number of variables which may be estimated with a reasonable resolution is limited in identification analyses by the information contained in the experimental or observational data. Recognition of the most consequential parameters is therefore essential. The selected model parameters consist of: (1) material elasticity coefficients of shear modulus and Poisson's ratio (G_0 and v), and (2) plasticity variables ($f, M, \boldsymbol{\alpha}, a, \boldsymbol{\mu}, \mathbf{P}$, and H_p). The initial conditions may reasonably be considered to correspond to rest, and the mass density may be measured accurately in laboratory or *in situ*. The boundary conditions are not required in local identifications using the developed technique.

Analyses of uniaxial constitutive relations suggest that the elastic and plastic moduli are the most consequential phenomenological parameters that control a stress–strain response. Furthermore, an accurate description of the plastic modulus upon unloading and reloading in a different direction, is essential in modelling a dynamic constitutive behaviour. The modulus H_p, which may be expressed as follows (by combining the flow rule and loading function):

$$H_p = \frac{\mathbf{Q} : \mathrm{d}\boldsymbol{\sigma}'}{\mathbf{P} : \mathrm{d}\boldsymbol{\varepsilon}^p} \tag{23}$$

plays the role of plastic modulus for multidimensional stress conditions. This modulus is also given by [18]:

$$H_p = -\frac{a\partial f/\partial \boldsymbol{\alpha} : \boldsymbol{\mu} + b\partial f/\partial M}{\|\partial f/\partial \boldsymbol{\sigma}\|} \tag{24}$$

These two equations show clearly that the variations of the plastic modulus are a direct function of the yield relationship, the plastic internal variables, the flow rule, and hardening rules of the plastic internal variables. Calibration of a constitutive model using the plastic modulus as main parameter is basically equivalent to an identification analysis based the yield, flow and hardening parameters. The former is only more convenient.

The plastic modulus, H_p, of the soil models described above is directly related to the usual soil shear modulus. For clayey soils, this modulus reduces to: $H_p = 2(1/G - 1/G_0)^{-1}$, where G_0 and G are elastic and tangent shear moduli. Similarly, for a cohesionless soil under triaxial loading conditions with constant effective confining pressure, $p' = p_c$, the plastic modulus is given by

$$H_p = 2\left[\left(\frac{1}{G} - \frac{1}{G_0}\right)\left(1 + \frac{\mathbf{S}' : \mathbf{S}'}{3p_c^2}\right)\right]^{-1} \tag{25}$$

The elastic and tangent shear moduli, G_0 and G, and the damping factor, ζ, along with the volumetric flow relation (Eq. (22)) for cohesionless media, are therefore the set of fundamental phenomenological parameters that control the behaviour of soils. Poisson's ratio variations were assumed to be insignificant under short term dynamic loading conditions.

3.4. Estimation of accelerations

The computed stresses and recorded pore pressures were employed, along with the equilibrium equations, to evaluate the accelerations, $\ddot{\mathbf{u}}^{(m)}$, associated with the selected class of constitutive models:

$$\ddot{\mathbf{u}}^{(m)} = \frac{1}{\rho}(\boldsymbol{\sigma}' + p_w\boldsymbol{\delta}) \cdot \boldsymbol{\nabla} + \mathbf{g} \tag{26}$$

A discrete counterpart of Equation (26) within the ξ_i skew rectilinear co-ordinate system was used to evaluate the accelerations at the (p, q, r) central location of a parallelepiped instrument configuration (Figures 4 and 6), which correspond to the computed stresses $\boldsymbol{\sigma}_\xi = \boldsymbol{\Phi}^{-1}_{x-\xi}\boldsymbol{\sigma}\boldsymbol{\Phi}_{x-\xi}$ at the intermediate locations $(p - \frac{1}{2}, q - \frac{1}{2}, r - \frac{1}{2})$ to $(p + \frac{1}{2}, q + \frac{1}{2}, r + \frac{1}{2})$. When a cluster is larger than 3-by-3-by-3 accelerometers, accelerations may be evaluated at the location of all interior sensors (not located on an edge or a corner).

3.5. Model calibration

The selected class of models were calibrated utilizing a simple deterministic approach. Stiffness and damping parameters of the models described above were estimated using generalized (weighted) least-squares optimality criteria [20–22], so as to minimize the discrepancy between observed (recorded) acceleration time histories, $\ddot{\mathbf{u}}^{(o)}$, and those predicted by the selected models, $\ddot{\mathbf{u}}^{(m)}$, at the central location (p, q, r). The optimality criterion is given by

$$\mathcal{O} = \int_0^T \|\ddot{\mathbf{u}}^{(o)} - \ddot{\mathbf{u}}^{(m)}\|_{\mathbf{W}}\, \mathrm{d}t + \|\mathbf{p} - \mathbf{p}^{(a)}\|_{\mathbf{W}_p} \tag{27}$$

in which T is time length of observations, $\|\ddot{\mathbf{u}}^{(o)} - \ddot{\mathbf{u}}^{(m)}\|_{\mathbf{W}}$ refers to the weighted Euclidean norm of $\ddot{\mathbf{u}}^{(o)} - \ddot{\mathbf{u}}^{(m)}$, $\mathbf{W}$ is a positive definite weighting matrix which takes into account the available information regarding the model performance [22], $\mathbf{p}$ refers collectively to the stiffness and damping parameters described above, $\mathbf{p}^{(a)}$ is *a priori* estimate of $\mathbf{p}$, and $\mathbf{W}_p$ is an associated weighting matrix. The term $\|\mathbf{p} - \mathbf{p}^{(a)}\|_{\mathbf{W}_p}$ reflects the uncertainty and confidence level in the *a priori* parameter estimates, and is used to improve the problem conditioning [22,23]. The model optimal parameters are then given by: $\min_{\mathbf{p}>\mathbf{0}} \mathcal{O}$. This deterministic approach, which was adopted in view of its simplicity, does have an underlying equivalent probabilistic model [24].

A general functional was pre-selected for the shear modulus based on expected variations for soil media [25]:

$$G(\boldsymbol{\gamma}) = \frac{G_0 - G_p}{(1 + (\frac{\gamma}{\gamma_0})^n)^{(n+1)/n}} + G_p \tag{28}$$

in which G_0 and G_p are initial and large-strain moduli and, γ_0 and n are parameters defining the variations as a function of shear strain amplitude, γ. Thus, the identification is reduced to an estimation of G_0, G_p, γ_0, n, $\bar{\eta}$, and ζ. The numerical evaluation of optimal parameters was performed using quasi-Newton non-linear optimization techniques [26,27]. Non-constrained algorithms were employed using a logarithmic change of variables.

4. COMPUTER SIMULATIONS AND VERIFICATION

Analytical investigation of convergence and accuracy of the developed identification technique is feasible only for the simple case of linear elastic systems. For these systems, uniqueness of the identification problem solution may be demonstrated for noise free acceleration and pore pressure records. Such analyses are not possible for a more realistic elasto-plastic 2-phase soil model (Eq. (21)). The proposed identification technique was therefore assessed using computer simulations. The conducted investigations were specifically aimed at analysing convergence properties and impact of discretization errors. Finite difference and finite element computational simulations were used to generate synthetic seismic records of the soil-retaining wall system of Figure 8. Soil behind the retaining-wall consisted of water saturated cohesionless granular strata, which are characterized by the constitutive model given by Equations (17)–(22) and marked by the presence of a weak layer. The synthetic accelerations of this layer in the retaining-wall vicinity and the free-field (Fig. 8) were used to demonstrate the developed technique capabilities in capturing local response characteristics and properties.

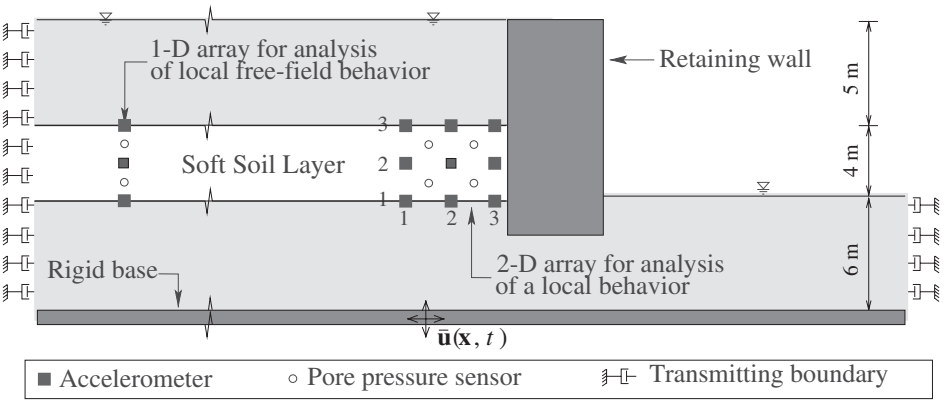

Figure 8. Configuration of soil-retaining wall model used in numerical simulations.

4.1. Verification

Numerical investigations were employed first to examine the consistency of the developed discrete (finite difference) local analysis algorithm (Sections 3.2–3.4) with the associated boundary value problem (Section 2). Using the actual soil model and properties, estimates of the weak layer accelerations using the developed local technique (Equation (26)) were found, as expected, to be identical to those that were evaluated based on a finite-difference solution of the global boundary value problem of the soil-retaining wall system (Equations (1)–(9)).

Thereafter, local 2-D identification analyses of the weak layer were conducted using the synthetic response of a finite element model. The records (synthetic response) provided by an array of a 3-by-3 accelerometers (separated by 2 m laterally and vertically), and 4 pore pressure sensors (at the intermediate central locations of the accelerometer array, Figure 8) were employed to identify soil response properties behind the retaining wall. The synthetic accelerations along the central vertical array (i.e. at locations $(2,1)$, $(2,2)$ and $(2,3)$) and pore pressure at the intermediate central points $(2\frac{1}{2}, 1\frac{1}{2})$ and $(2\frac{1}{2}, 2\frac{1}{2})$ are displayed in Figure 9. The recorded (simulated) and identified accelerations at the central location $(2,2)$ of the instrument array were found to be in good agreements (Figure 10). Close agreements were also obtained between the estimated and actual shear modulus variations with strain amplitude. Note that no *a priori* information was used in these analyses as $\mathbf{W}_p$ was set to the zero matrix. Errors were generally of the order of 1.5% or less for the shear modulus variables (Equation (28)) and less than 0.5% for the dilation parameter $\bar{\eta}$ (Equation (22)). These errors reflected the impact of discretization errors associated with the finite element (used in generating synthetic data) and

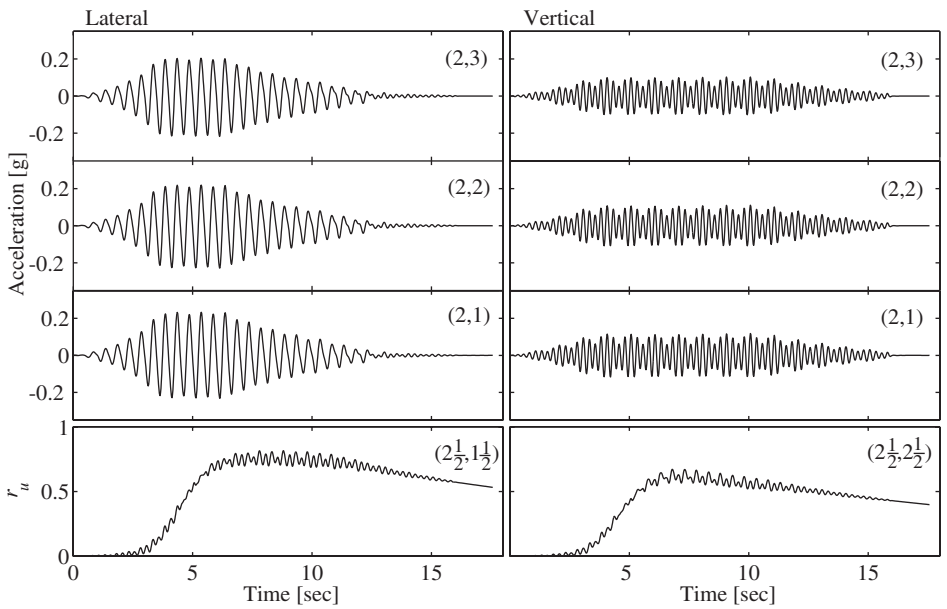

Figure 9. Recorded (simulated) accelerations and pore water pressure ratios (r_u) of the soil-retaining wall system of Figure 8.

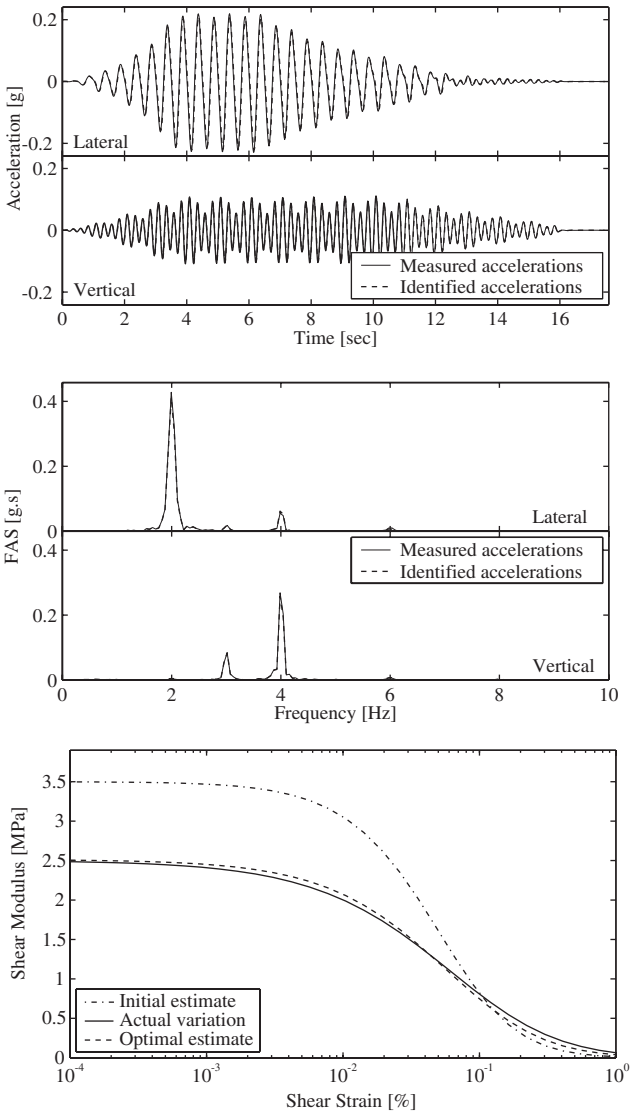

Figure 10. Local identification of the soil-retaining wall (finite element) model of Figure 8: acceleration time histories, Fourier amplitude spectra (FAS), and shear moduli at the (2, 2) central instrument location.

finite difference (used in local identification) techniques. Figure 11 shows the optimal shear stress–strain history at the $(2\frac{1}{2}, 1\frac{1}{2})$ location of the employed 2-D array behind the retaining wall (Figure 8), and corresponding history at the nearest finite element integration point. These two histories present the same response patterns. The observed discrepancies are associated mostly with the difference in induced strains at these 2 different locations (which are separated by a distance of about 0.4 m).

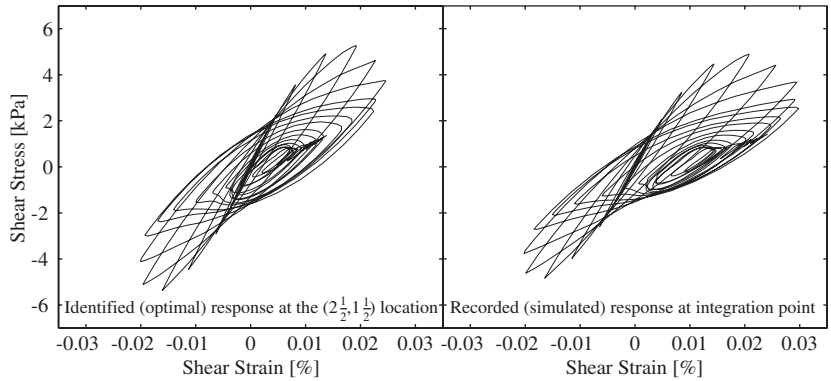

Figure 11. Optimal shear stress–strain history at the $(2\frac{1}{2}, 1\frac{1}{2})$ location behind the retaining wall of Figure 8 and corresponding history at the nearest finite element integration point.

4.2. Accuracy

Accuracy of the developed identification technique depends on the characteristics of involved system response and implementation details of the algorithm.

Permanent deformation. The response of soil systems is often marked by the appearance of permanent displacements and deformation when subjected to moderate or strong dynamic excitations. However, double time integration of acceleration records usually provides accurate estimates of only cyclic displacements. A number of numerical simulations were conducted to assess the impact of using only the cyclic component of strains (Section 3.2) on the proposed local identification analyses. These simulations revealed that neglecting the permanent components does not lead to significant errors in identified constitutive parameters if the amplitude of permanent strains is of the same order or less than that of cyclic components. New miniature sensing devices capable of measuring permanent displacements will be available in the near future e.g. Reference [28], and the evaluation of permanent strains will become a non-issue.

Response wave-length. The conducted analyses revealed that the solution to the identification problem exhibits sensible errors when the accelerometer spacings become significant. Discrepancies due to aliasing lead to sensible errors in strain estimates, unbalanced stresses, and a drift in computed accelerations when these spacings are higher than about 1/20 of involved wave lengths (i.e. higher than about 4 m for the system of Figure 8). These errors are reduced substantially when higher order interpolations or discrete differentiations are employed (e.g. using a 5-by-5 array of instruments for a 2-D analysis).

Algorithm. Alternative implementation schemes of the local identification technique were employed to assess the impact of the central acceleration records (of the instrument array) which are used in strain evaluation (Section 3.2) as well as in model calibration (Section 3.5). Figure 12 sketches a scheme (for a 2-D analysis) that uses the motion recorded by the central accelerometer only in model calibration. Identifications using this scheme were found to be in close agreement with those conducted using the original algorithm (Figure 7). Slight discrepancies were observed, and reflected the impact of instrument spacing and location on the evaluated strains (Section 3.2) and accelerations (Section 3.4) using finite differentiation techniques.

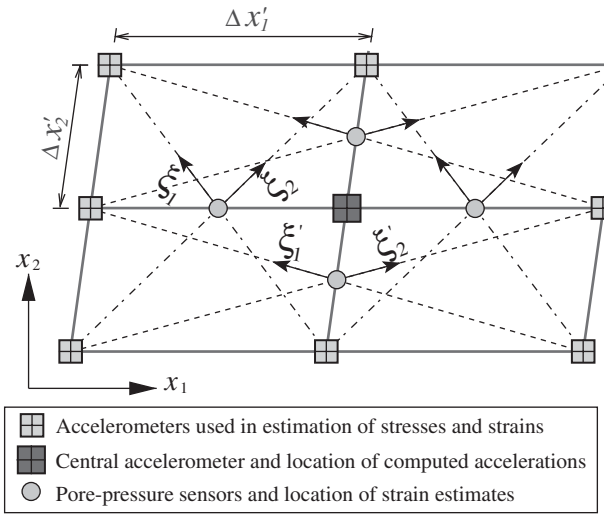

Figure 12. Alternative scheme of the local identification technique which uses the motion recorded by the central accelerometer in model calibration only (Section 3.5).

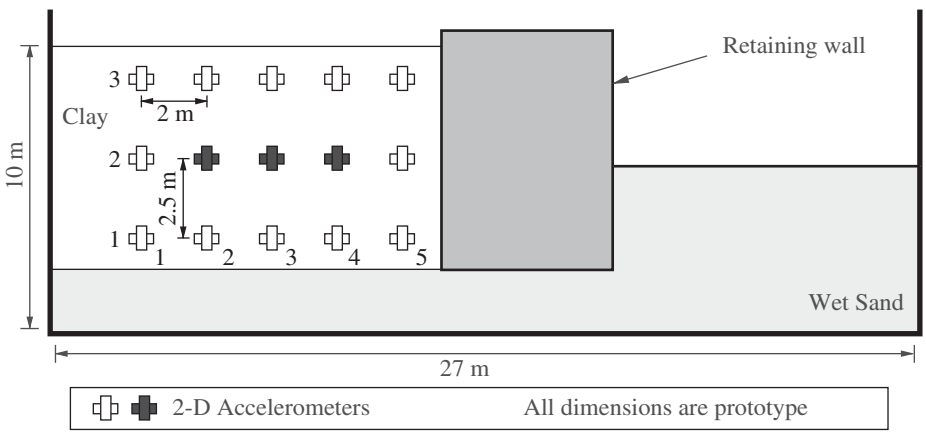

Figure 13. Configuration of analysed soil-retaining wall centrifuge model.

5. CENTRIFUGE MODEL ANALYSES AND VALIDATION

Centrifuge tests of a soil-retaining structure system were conducted in a rigid box under a 50 g gravity field (Figure 13) at Rensselaer. Soil consisted of a water saturated Georgia Kaolinite clay layer (with a Plasticity Index PI = 10%) overlying well-compacted wet Nevada sand (having a relative density $D_r = 70\%$). One-dimensional lateral shaking was imparted along the model base using an electro-hydraulic shaker. The 2-D response of the clayey soil was monitored at 15 locations behind the retaining structure using a 5×3 array of accelerometers (Figure 13). The recorded accelerations provided ample experimental data to locally assess the constitutive stress–strain relationship of the clay layer using the developed second order accurate algorithm.

Fig. 14 shows the recorded and computed (optimal) acceleration time histories as well as Fourier amplitude spectra at the (4,2) location within the clay layer when subjected to a low amplitude excitation. This excitation induced mostly a linear response, and the estimated low-strain shear modulus ($G_0 = 3.3$ MPa) was found to be in close agreement with the modulus estimated based on a non-parametric 1-D shear stress–strain [16] analysis ($G_0 = 3.6$ MPa) using only the lateral motion of the vertical array composed of accelerometers at the $(4, 1)$, $(4, 2)$, and $(4, 3)$ locations.

The soil-retaining wall system was thereafter subjected to a series of base excitations with increasing amplitudes. Figure 15 exhibits soil accelerations recorded by the second and fourth vertical arrays (of accelerometers at the $(2, 1)$, $(2, 2)$, and $(2, 3)$, and $(4, 1)$, $(4, 2)$, and $(4, 3)$ locations) under a base acceleration having a peak amplitude of the order of 0.4 g. The identified accelerations at $(4, 2)$ are shown in Figure 16, along with the corresponding shear modulus variation with strain amplitudes. Good agreements were obtained between computed and recorded accelerations at this $(4, 2)$ location, as well as at $(2, 2)$ and $(3, 2)$. The estimated low strain viscous damping was of the order of 3%, which is within the general range of values obtained for clayey soils based on sample testing [29].

Figure 17 depicts the optimal stress strain histories at the $(4, 1\frac{1}{2})$ and $(2, 1\frac{1}{2})$ locations along with the corresponding histories obtained using an approximate non-parametric 1-D stress–

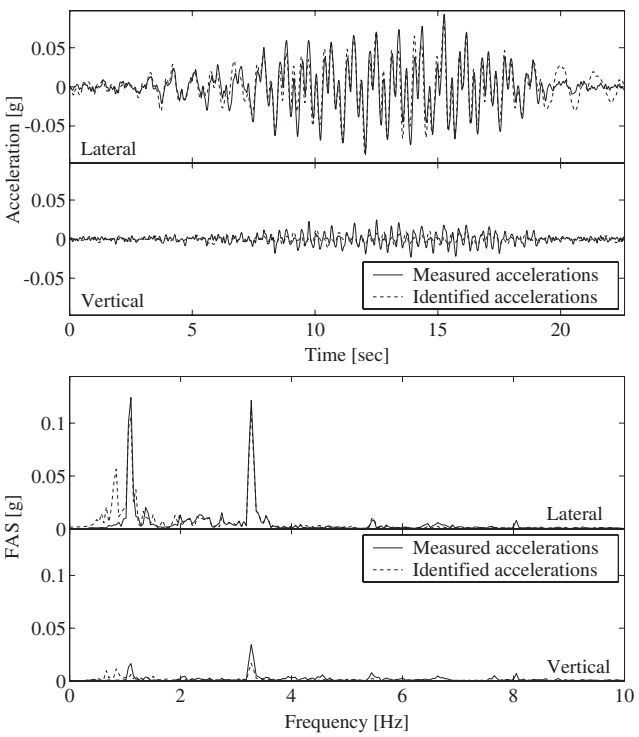

Figure 14. Local identification of the soil-retaining wall centrifuge model of Figure 13 when subjected to a low-amplitude shaking: acceleration time histories and Fourier amplitude spectra (FAS) at the $(4, 2)$ instrument location.

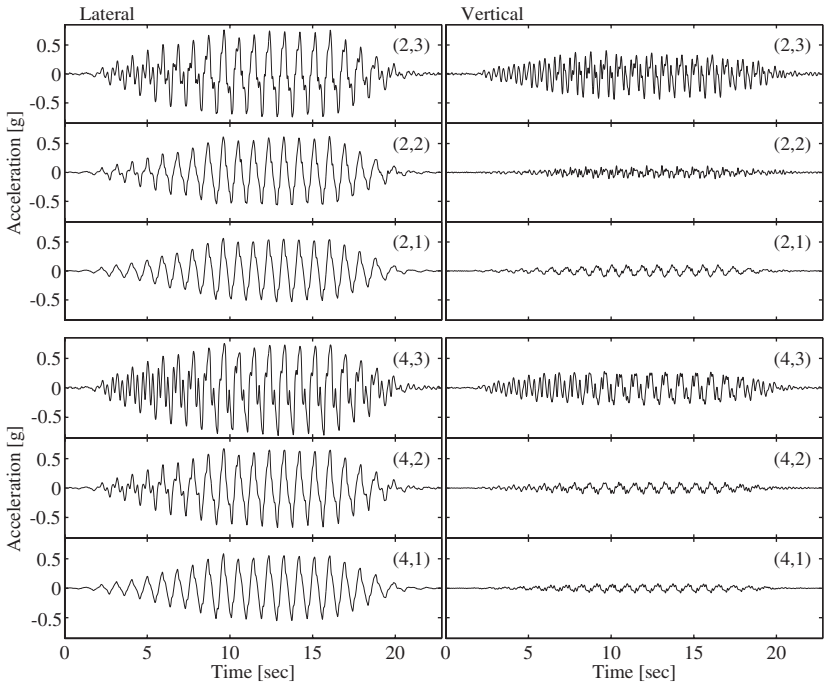

Figure 15. Recorded accelerations along the second and fourth vertical arrays (i.e. at the (2, 1), (2, 2) and (2, 3), and (4, 1), (4, 2) and (4, 3) locations) of the cluster of instruments of Figure 13.

strain analysis [16]. This approximate analysis neglects the normal lateral stresses and assumes that the soil lateral response is fully described by a shear beam idealization. Significant discrepancies in stresses and stiffness properties are observed between these two estimates. The non-parametric 1-D stress–strain analysis was therefore modified to take into account the impact of lateral normal stresses. The simple shear beam idealization was coupled with a Winkler spring model with a stiffness coefficient estimated using a simple 1-D analysis of lateral normal wave propagations (more details are provided in Reference [30]). The stress–strain histories provided by this modified approach are found to be in good agreements with those identified using the developed local algorithm. The variations of shear moduli evaluated based on these two techniques were consistent (Figure 16).

6. CONCLUSIONS

A local system identification technique was developed to investigate the constitutive behaviour of distributed geotechnical and geophysical systems. Local mechanisms of soil response were analysed using acceleration and pore pressure records provided by a cluster of closely spaced instruments. The developed technique does not require the availability of boundary condition measurements, or solution of a boundary value problem associated with an observed system. Such an approach is particularly advantageous in investigations of the seismic response of semi-

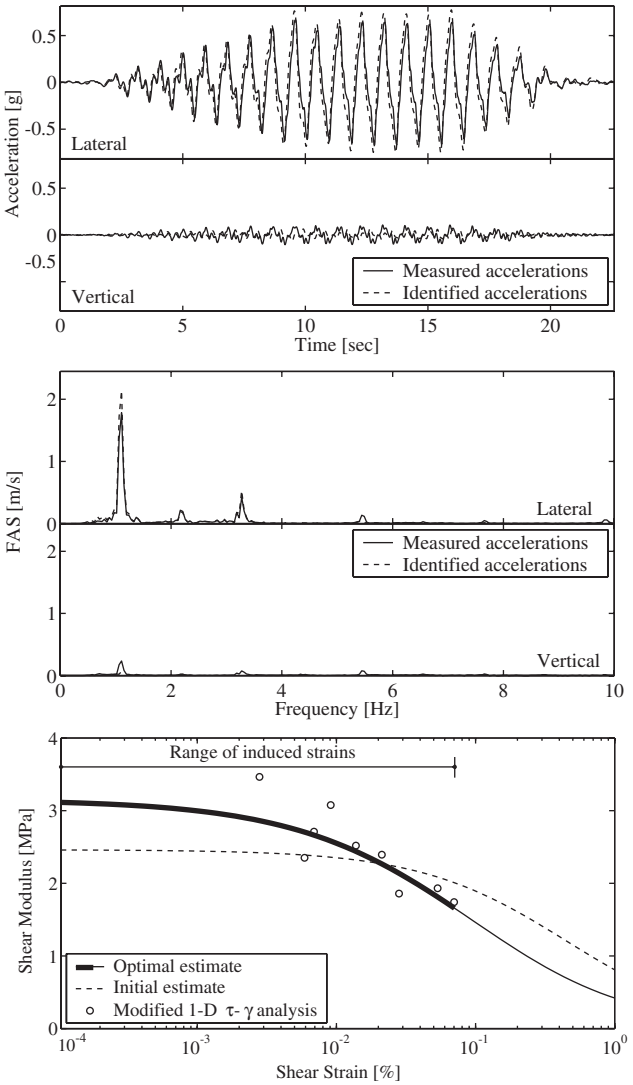

Figure 16. Local identification of the retaining wall–soil centrifuge model of Figure 13 when subjected to a strong shaking: acceleration time histories, Fourier amplitude spectra (FAS), and shear moduli at the (4, 2) instrument location.

infinite systems, as well as in the presence of local mechanisms. Global identifications based on boundary value problem formulations generally smear the effects of local mechanisms and may lead to erroneous results. Computer simulations and centrifuge tests of a soil-retaining wall system were used to assess the capabilities of the developed technique. The conducted analyses showed that local system identification provides an effective means to analyse the constitutive behaviour of a complex distributed soil system at specific locations independently of adjacent response mechanisms or material properties.

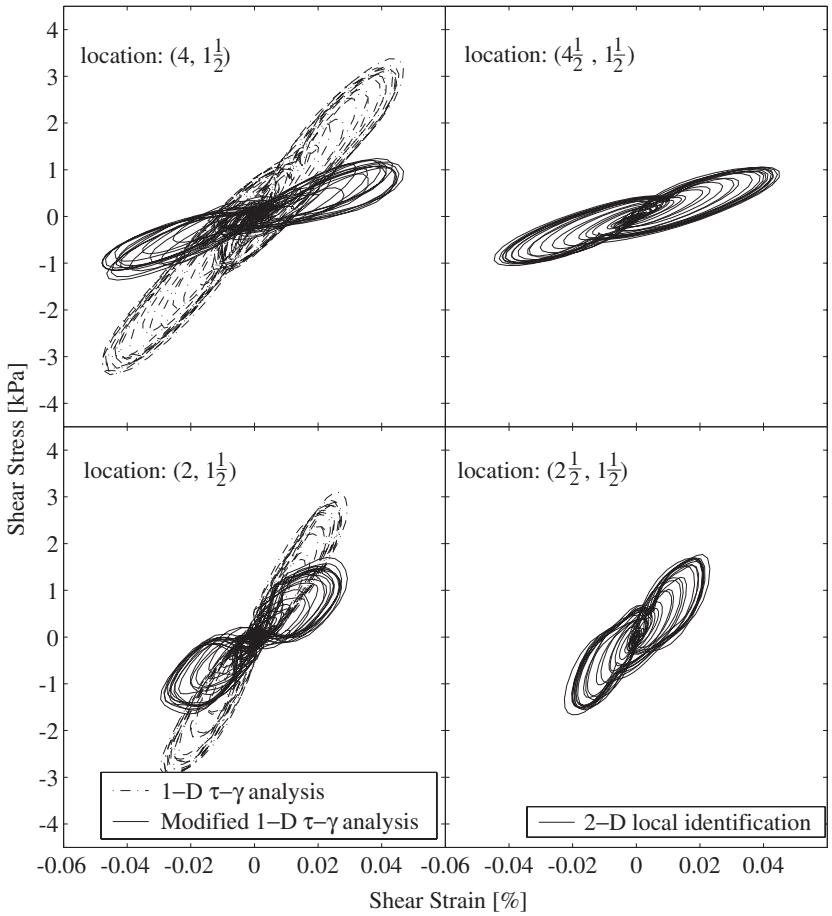

Figure 17. Shear stress–strain histories of the centrifuge soil-retaining wall system of Figure 13 evaluated using the developed local identification technique along with those obtained using a simple and a modified 1-D analysis.

ACKNOWLEDGEMENTS

This research was supported by the National Science Foundation, Grant No. CMS-9984754 (Dr. Cliff Astill program manager). This support is gratefully acknowledged.

REFERENCES

1. National Research Council. *Liquefaction of Soils During Earthquakes*. Committee on Earthquake Engineering: Washington, DC, 1985.
2. Arulanandan K, Scott RF (eds). *Verification of Numerical Procedures for the Analysis of Soil Liquefaction Problems*, vol 1. Balkema: Davis, CA, 1993.
3. Ishihara K. *Soil Behaviour in Earthquake Geotechnics*. Oxford University Press: New York, 1996.
4. Zienkiewicz OC, Chan AHC, Pastor M, Schrefler BA, Shiomi T. *Computational Geomechanics with Special Reference to Earthquake Engineering*. Wiley: England, 1998.
5. Scott RF. Lessons learned from velacs project. In *Proceedings of International Conference on the Verification of Numerical Procedures for the Analysis of Soil Liquefaction Problems*, Davis UC, Arulanandan K, Scott RF (eds). A.A. Balkema: Rotterdam, The Netherlands, October 17–20, 1994; 1773–1784.

6. Wood C, Copeland D, Viksne A. Strong motion data, loma prieta earthquake of October 17, 1989, san justo dam and dike, san luis dam, o'neill forebay dam, martinez dam. *Technical Report*, U.S. Department of the Interior, Bureau of Reclamation, Denver, Colorado, 1991.
7. Zeghal M, Elgamal A-W. Site response and vertical seismic arrays. *Progress in Structural Engineering and Materials* 2000; **2**(1):92–101 (Invited article).
8. Elgamal A, Lai T, Yang Z, He L. Dynamic soil properties, seismic downhole arrays and applications in practice. In *Proceedings of the Fourth International Conference on Recent Advances in Geotechnical Earthquake Engineering and Soil Dynamics and Symposium in Honor of Professor W. D. Liam Finn*, Prakash S (ed.). Number SOAP-6, San Diego, California, March 26–31, 2001 (State-of-the-art paper).
9. Oskay C, Zeghal M. *Geotechnical System Identification*: *a Survey*, 2003, submitted for publication.
10. D.C. Greene, Sensor technology and applications to a real-time monitoring system. *M.S. Thesis*, Massachusetts Institute of Technology, 2001.
11. Prime Faraday Partnership. *An Introduction to MEMS* (*Micro-electromechanical Systems*). Wolfson School of Mechanical and Manufacturing Engineering, Loughborough University: Loughborough, England, 2002.
12. Prevost JH. Mechanics of continuous porous media. *International Journal of Engineering Science* 1980; **18**(5): 787–800.
13. Lapidus L, Pinder GF. *Numerical Solution of Partial Differential Equations in Science and Engineering*. Wiley: New York, 1982.
14. Pearson EC. *Numerical Methods in Engineering and Science*. Van Nostrand Reinhold: New York, 1986.
15. Eringen AC. *Mechanics of Continua*. Wiley: New York, 1967.
16. Zeghal M, Elgamal A-W, Tang HT, Stepp JC. Lotung downhole seismic array: evaluation of soil nonlinear properties. *Journal of Geotechnical Engineering*, *ASCE* 1995; **121**(4):363–378.
17. Prevost JH. Modeling the behaviour of geomaterials. In Sayed SM (ed.). *Geotechnical Modeling and Applications*, Gulf Publishing Company: Houston, 1987.
18. Prevost JH. A simple plasticity theory for frictional cohesionless soils. *Soil Dynamics and Earthquake Engineering* 1985; **4**(1):9–17.
19 Elgamal AW, Zeghal M, Parra E, Gunturi R, Tang HT, Stepp JC. Identification and modelling of earthquake ground response i: site amplification. *Soil Dynamics and Earthquake Engineering* 1996; **15**:499–522.
20. Bard Y. *Nonlinear Parameter Estimation*. Academic Press: New York, 1974.
21. Tarantola A, Valette B. Generalized nonlinear inverse problems solved using the least squares criterion. *Reviews of Geophysics and Space Physics* 1982; **20**(2):219–232.
22. Tarantola A. *Inverse Problem Theory*. Elsevier: Amsterdam, 1987.
23. Tikhonov AN, Arsenin VY. *Solutions of Ill-Posed Problems*. Winston: Washington, 1977.
24. Mohammad-Djafari A. From deterministic to probabilistic approaches to solve inverse problems. In *Bayesian Inference for Inverse Problems*, SPIE 98: San Diego, CA, U.S.A., 1998; 2–11.
25. Richard RM, Abbott BJ. Versatile elastic–plastic stress–strain formula. *Journal of the Engineering Mechanics Division* 1975; **101**:511–515.
26. Gill PE, Murray W, Wright MH. *Practical Optimization*. Academic Press: New York, 1981.
27. Dennis JE, Schnabel RB. *Numerical Methods for Unconstrained Optimization and Nonlinear Equations*. Prentice-Hall: Englewood Cliffs, NJ, 1983.
28. Measurand Inc. ShapeTape. *http://www.measurand.com/products/shapetape.html*, 2003.
29. Vucetic M, Dobry R. Effect of soil plasticity on cyclic response. *Journal of Geotechnical Engineering* 1991; **117**(1): 89–107.
30. Oskay C. Local identification analyses of soils and soil-structure systems. *Ph.D. Thesis*, Rensselaer Polytechnic Institute, Troy, New York, January 2003.

